SSC23-XI-03

Drag-Based Formation Control of Millennium Space Systems Satellites

Sanny Omar
Millennium Space Systems
2265 E. El Segundo Blvd, El Segundo, Ca 90245
sanny.omar@millennium-space.com

ABSTRACT

Aside from gravity, aerodynamic drag is typically the strongest environmental force acting on a spacecraft in low Earth orbit. While often treated as a disturbance whose perturbative effects on the orbit must be mitigated through periodic thruster burns, drag can potentially be harnessed for on-orbit maneuvering.

This paper discusses a practical algorithm for achieving and maintaining a desired separation between two satellites using differential aerodynamic drag. By increasing the drag and thereby reducing the mean semi-major axis of "lead" vehicle, the separation between the satellites is increased. Conversely, by increasing the relative drag on the "chase" vehicle, inter-satellite separation is decreased. With this control concept, the derived algorithms compute how long each satellite should stay in either a minimum or maximum drag configuration and when the drag configurations should be changed.

Flight results are presented for two propellant-free vehicles operated by Millennium Space Systems where this drag control strategy was successfully applied to achieve a desired inter-satellite separation. Using open loop commands, ephemeris knowledge from freely available TLEs, and the ability to orient the primary solar arrays differently while in eclipse, mission operators were able to achieve a vehicle separation within the required tolerance with minimal drift over time.

INTRODUCTION

Many spacecraft missions require the establishment and maintenance of an along-track separation between two low Earth orbit (LEO) satellites initially deployed into the same orbit. This separation may be required for communication crosslinks, observations of terrestrial locations over time, or other operational or scientific reasons[1,2]. If the satellites in question are at low enough altitudes for aerodynamic drag to be significant, the satellites are capable of changing their attitudes, and the cross-sectional area of a given satellite relative to the velocity vector changes significantly based on attitude, the satellite operators can modulate the aerodynamic drag experienced by each satellite through attitude changes. The along-track separation between the satellites can then be controlled by modulating the drag force experienced by each satellite[3,4]. Though slower and less precise than traditional thruster-based control, differential drag control has the benefit of not requiring any propellant. Eliminating the propulsion system from a satellite design reduces satellite mass, complexity, and component costs, potentially resulting in savings of millions of dollars. Differential drag control can also be utilized to save fuel on satellites containing thrusters and can be implemented post-launch on satellites experiencing thruster system failures.

While some spacecraft operators such as PlanetLabs have used differential drag for spacecraft constellation control in the past[5], the majority of the publications in this field remain theoretical in nature and do not adequately address practical considerations such as vehicle operational constraints, operator command uplink cadence, orbit determination uncertainties, and aerodynamic uncertainties.

This paper first discusses the generalized differential drag control logic assuming two LEO satellites capable of holding either a minimum-drag or maximum-drag configuration. Simulation results of differential-drag control maneuvers are then presented showcasing the capabilities of this algorithm to work despite operational constraints such as the need to maintain a sun-pointing mode of operation while not in eclipse. The successful application of this theory to two space vehicles built by Millennium Space Systems, here called SV1 and SV2 is then discussed. Using existing attitude control logic and the different drag areas resulting from orienting the solar panel arrays perpendicular or parallel to the velocity vector, a desired inter-satellite separation was

established and maintained using exclusively differential aerodynamic drag forces. No additional software logic on the satellites was necessary to perform this maneuver, resulting in significant customer benefits for a minimal cost.

DRAG-INDUCED RELATIVE MOTION THEORY

The first step in developing the differential drag control algorithms involves deriving the equations that describe the relative motion of two satellites under the influence of differential aerodynamic drag. Define the difference in mean argument of latitude between two satellites as

$$\phi = M_1 - M_2 \tag{1}$$

Where M_1 is the mean argument of latitude of satellite 1 (the leader) and M_2 is the mean argument of latitude of satellite 2 (the chaser). Note that mean argument of latitude is the sum of mean anomaly and argument of perigee and is equal to the true anomaly in a perfectly circular orbit. Using mean argument of latitude instead of true anomaly helps make the algorithms more robust to perturbed, non-circular orbits. $\dot{\phi}$ can be written as the difference in mean motion (n) between the satellites as

$$\begin{aligned}\dot{\phi} = n_1 - n_2 &= \sqrt{\frac{\mu}{(a_1)^3}} - \sqrt{\frac{\mu}{(a_2)^3}} \\ &= \sqrt{\mu}\left(\frac{1}{(a_1)^{\frac{3}{2}}} - \frac{1}{(a_2)^{3/2}}\right)\end{aligned} \tag{2}$$

Where a is semi-major axis and μ is the Earth's gravitational parameter. Define

$$\delta = a_1 - a_2 \tag{3}$$

$\dot{\phi}$ can be written as

$$\dot{\phi} = \sqrt{\mu}\left((a_1)^{-3/2} - (a_1 - \delta)^{-3/2}\right) \tag{4}$$

From the binomial expansion theorem, for some small value x, the following relationship is true

$$\begin{aligned}(1+x)^n &= \sum_{k=0}^{n} \frac{n!}{k!\,(n-k)!} x^k \\ &\approx \frac{n!}{0!n!} + \frac{n!}{1!\,(n-1)!} x \\ &= 1 + nx\end{aligned} \tag{5}$$

Assuming that δ is small realtive to a_1, the term $(a_1 - \delta)^{-3/2} = (a_1)^{-3/2}(1 - \delta/a_1)^{-3/2}$ can be re-written using Eq. (5) as

$$\begin{aligned}&(a_1)^{-3/2}(1-\delta/a_1)^{-3/2} \\ &\qquad = (a_1)^{-3/2}\left(1 + \frac{3\delta}{2a_1}\right) \\ &\qquad = (a_1)^{-5/2}\left(a_1 + \frac{3\delta}{2}\right)\end{aligned} \tag{6}$$

Substituting Eq. (6) for $(a_1 - \delta)^{-3/2}$ in Eq. (4) yields

$$\begin{aligned}\dot{\phi} &= \frac{\sqrt{\mu}}{(a_1)^{5/2}}\left(a_1 - \left(a_1 + \frac{3\delta}{2}\right)\right) \\ &= \frac{-3\delta\sqrt{\mu}}{2(a_1)^{5/2}}\end{aligned} \tag{7}$$

Note that $a_a = (a_1 + a_2)/2$ can be used in place of a_1 for better accuracy in Eq. (7) yielding the following equation for the rate of change of mean argument of latitude separation between two satellites based on the difference in semi-major axis.

$$\dot{\phi} = \frac{-3\delta\sqrt{\mu}}{2(a_a)^{5/2}} \tag{8}$$

The next step is to compute the second derivative of ϕ with respect to time. Assuming a_a does not change significantly, we get

$$\frac{d^2\phi}{dt^2} = \ddot{\phi} \approx \frac{-3\sqrt{\mu}}{2(a_a)^{\frac{5}{2}}}\left(\frac{d\delta}{dt}\right) \tag{9}$$

From the work energy theorem, the time rate of change of orbital energy $\left(E = -\frac{\mu}{2a}\right)$ equals the rate at which work is done by aerodynamic drag. If a_d is the acceleration due to drag and v is the orbital velocity, the rate at which work is done by aerodynamic drag is $-a_d v$ so

$$-a_d v = \frac{dE}{dt} = \frac{\mu}{2a^2}\frac{da}{dt} \tag{10}$$

Note that in an approximately circular orbit

$$v = \sqrt{\frac{\mu}{a}} \tag{11}$$

$$a_d = C_b \rho v^2 = \frac{C_b \rho \mu}{a} \tag{12}$$

Where

$$C_b = \frac{C_d A}{2m} \tag{13}$$

is the spacecraft ballistic coefficient and ρ is atmospheric density. Solving Eq. (10) for $\frac{da}{dt}$ and substituting Eq. (12) for a_d yields

$$\frac{da}{dt} = -\frac{2a_d v a^2}{\mu} = -2C_b \rho \sqrt{\mu a} = -2B^* \sqrt{\mu a} \tag{14}$$

$$\frac{d\delta}{dt} = \frac{da_1}{dt} - \frac{da_2}{dt} \approx -2\sqrt{\mu a_a}(B_1^* - B_2^*) \tag{15}$$

Where $B^* = C_b \rho$. Substituting Eq. (15) into Eq. (9) yields

$$\ddot{\phi} = \frac{3\mu}{a^2}(B_1^* - B_2^*) \tag{16}$$

With knowledge of B_1^*, B_2^*, a_1, and a_2 and the use of Eq. (8) and Eq. (16), it is possible to compute $\dot{\phi}$ and $\ddot{\phi}$. Using these computations, knowledge of the initial ϕ_0, and a desired final ϕ_d, the drag profile required for each satellite in order to achieve ϕ_d can be computed.

SEPARATION CONTROL STRATEGY USING DIFFERENTIAL DRAG

Consider the case where satellite 1 and satellite 2 start at identical a with some initial separation ϕ with sat 1 ahead and the goal is to bring them closer together. Each satellite can maintain either a minimum drag or a maximum drag configuration. In this scenario, sat 2 must begin in max drag and sat 1 in min drag (negative $\ddot{\phi}$). After time t_s, sat 2 is set to min drag and sat 1 to max drag (positive $\ddot{\phi}$). After time t_r, both satellites arrive at the same a ($\ddot{\phi} = 0$) and are set to a minimum or nominal drag configuration. If the goal is to increase ϕ, sat 1 begins in max drag and sat 2 in min drag (positive $\ddot{\phi}$) with a configuration swap at t_s for negative $\ddot{\phi}$ and a return to the same a at time t_r. If the satellites are not initially at the same semi-major axis, the sign of the initial $\ddot{\phi}$ is determined based on the resulting ϕ if drag is used to bring satellites to same a as soon as possible. If ϕ upon return to a common a is less than desired, the initial $\ddot{\phi}$ must be positive. Conversely, a negative initial $\ddot{\phi}$ is required if ϕ upon return to common a is greater than desired. Figure 1 illustrates the drag configurations required for a maneuver to bring two satellites closer together.

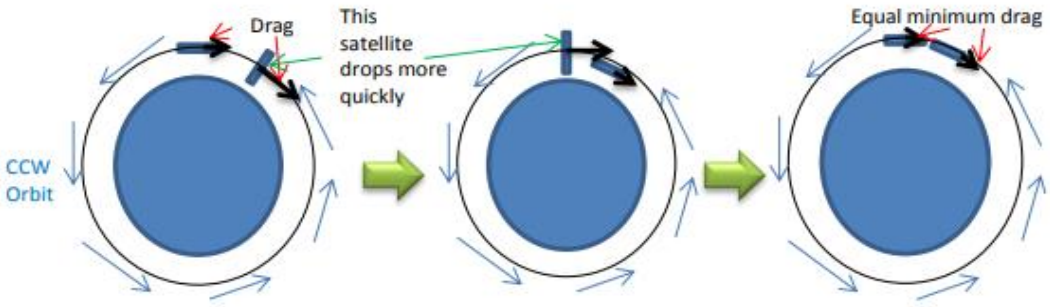

Figure 1. Differential Drag Maneuver Schematic

All differential drag maneuvers will have the following format:

1. $\ddot{\phi}_1$ maintained until time t_s (phase 1)
2. $\ddot{\phi}_2$ maintained until time t_r (phase 2)
3. Satellites set to same drag configuration for $\ddot{\phi} = 0$ at t_r

$\ddot{\phi}_1$ and $\ddot{\phi}_2$ are determined using Eq. (16) and the minimum and maximum B^* values achievable by each satellite. The remainder of the algorithms involve the calculation of t_s and t_r. Once these values are computed, the corresponding drag profiles can be commanded open loop.

First, the initial $\dot{\phi}_{10}$ is computed based on the initial $\delta_0 = a_{10} - a_{20}$ and Eq. (8). The change in ϕ that occurs during phase 1 (t_0 to t_s) can be computed by

$$\Delta\phi_1 = \dot{\phi}_{10} t_s + \frac{1}{2}\ddot{\phi}_1 t_s^2 \tag{17}$$

The change in ϕ that occurs during phase 2 (t_s to t_r) is computed by

$$\Delta\phi_2 = \dot{\phi}_{20} t_r + \frac{1}{2}\ddot{\phi}_2 t_r^2 \tag{18}$$

$$\dot{\phi}_{20} = \dot{\phi}_{10} + \ddot{\phi}_1 t_s \tag{19}$$

Where $\dot{\phi}_{20}$ is the rate of change of ϕ at the swap time. The desired change in ϕ achieved by the end of the maneuver ($\Delta\phi_t$) is given by

$$\Delta\phi_t = \Delta\phi_1 + \Delta\phi_2 \tag{20}$$

Because we want zero drift rate between the satellites at the end of the maneuver, we have a final separation rate given by

$$\dot{\phi}_t = 0 = \dot{\phi}_{10} + \ddot{\phi}_1 t_s + \ddot{\phi}_2 t_r \tag{21}$$

We now have 5 equations (Eq. (17) – Eq. (21)) and 5 unknowns ($\Delta\phi_1, \Delta\phi_2, \dot{\phi}_{20}, t_s, t_r$). t_s and t_r can be solved for as follows. From Eq. (21),

$$t_r = -\frac{\dot{\phi}_{10} + \ddot{\phi}_1 t_s}{\ddot{\phi}_2} \tag{22}$$

Substituting Eq. (22) and Eq. (19) into Eq. (18) gives

$$\begin{aligned}\Delta\phi_2 = &-\frac{\left(\dot{\phi}_{10} + \ddot{\phi}_1 t_s\right)^2}{\ddot{\phi}_2} \\ &+ \frac{1}{2}\frac{\left(\dot{\phi}_{10} + \ddot{\phi}_1 t_s\right)^2}{\ddot{\phi}_2} \\ &= -\frac{\left(\dot{\phi}_{10} + \ddot{\phi}_1 t_s\right)^2}{2\ddot{\phi}_2}\end{aligned} \tag{23}$$

Substituting Eq. (23) and Eq. (17) into Eq. (20) gives

$$\begin{aligned}\Delta\phi_t = &\dot{\phi}_{10} t_s + \frac{1}{2}\ddot{\phi}_1 t_s^2 \\ &- \frac{\left(\dot{\phi}_{10} + \ddot{\phi}_1 t_s\right)^2}{2\ddot{\phi}_2}\end{aligned} \tag{24}$$

Eq. (24) can be put into quadratic form and then solved using the quadratic formula.

$$\begin{aligned}0 = &\left(-\ddot{\phi}_1^2 + \ddot{\phi}_1\ddot{\phi}_2\right)t_s^2 + \left(2\dot{\phi}_{10}\left(\ddot{\phi}_2 - \ddot{\phi}_1\right)\right)t_s \\ &+ \left(-\dot{\phi}_{10}^2 - 2\ddot{\phi}_2\Delta\phi_t\right) \\ &= a_q t_s^2 + b_q t_s + c_q\end{aligned} \tag{25}$$

Recognizing that a_q (the coefficient of t_s^2) is always negative because $\ddot{\phi}_1$ and $\ddot{\phi}_2$ have opposite signs and that t_s must be positive, we get

$$t_s = \frac{-b_q - \sqrt{b_q^2 - 4a_q c_q}}{2a_q} \tag{26}$$

Once t_s is computed, t_r can be found using t_s and Eq. (22). With the ability to compute t_s and t_r, the complete differential drag control algorithms proceeds according to the following steps:

- Simulate both satellites for 1 orbit to compute the average B^* term in min drag profile, max drag profile, and cruise profile
  - Simulation allows drag changes from attitude switches in eclipse to be captured
  - $B^* = \frac{\rho C_d A}{2m} = \rho C_b$
- Compute initial $\delta = a_1 - a_2$ and $\dot{\phi}_0$ based on difference in orbit-averaged mean semi-major axis between satellites
- Determine values of $\ddot{\phi}_1$ and $\ddot{\phi}_2$ based on initial conditions and desired final separation ϕ_{td}
- Estimate t_s and t_r based on analytical solution
- Propagate trajectory with $\ddot{\phi}_1$ until t_s and $\ddot{\phi}_2$ until return to same mean a (close to t_r)
- Compute difference between actual and desired ϕ at trajectory end
  - $\phi_e = \phi_{td} - \phi_{ta}$
- Compute $\phi_{aim} = \phi_{td} + \phi_e$
- Compute t_s and t_r needed to achieve ϕ_{aim} and propagate new trajectory
- Continue to update ϕ_{aim} via $\phi_{aim_i} = \phi_{aim_{i-1}} + \phi_{e_i}$, compute t_s and t_r, and propagate trajectory until t_s found such that $|\phi_e| < tolerance$
- Uplink accurate C_{b1}, t_s, C_{b2}, and t_r commands to each satellite

- Every few days, C_{b1}, t_s, C_{b2}, and t_r can be re-computed using this algorithm and re-uplinked to the satellites.

SIMULATION RESULTS

The following simulation results are for two satellites in 434 km altitude, 52 degree inclined orbits with a 700 km initial separation. Both satellites were assumed to have a minimum and maximum ballistic coefficient (defined in Eq. (13)) of .00460 m^2/kg and .01143 m^2/kg respectively. Each satellite was assumed to be able to hold a minimum or maximum drag configuration only while in eclipse and maintain a sun-pointing configuration with an average ballistic coefficient of .00883 m^2/kg when in the sun. Satellite 1 was initialized with a semi-major axis 150 m lower than satellite 2 and was ahead of satellite 2 in the along-track direction. The difference in semi-major axis causes satellite 1 to be drifting further away from satellite 2 at the start of the maneuver. The goal of the maneuver was to establish a 400 km final separation between the satellites with zero drift rate. The simulation was conducted using a two-body gravity model to make it easier to see the variation in the orbital elements over time. For the analytical swap time and return time solutions, an orbit-averaged minimum drag ballistic coefficient and orbit-averaged maximum drag ballistic coefficient value were used. In the numerical simulation, the change in ballistic coefficient as the satellite went from sunlight to eclipse was taken into account as shown in Figure 2 and Figure 3.

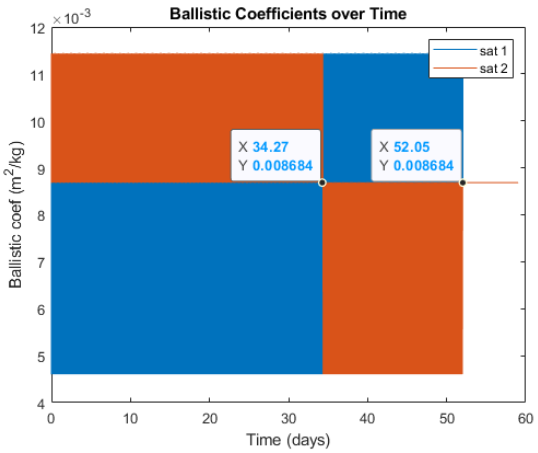

Figure 2. Ballistic Coefficients over Time during Differential Drag Maneuver

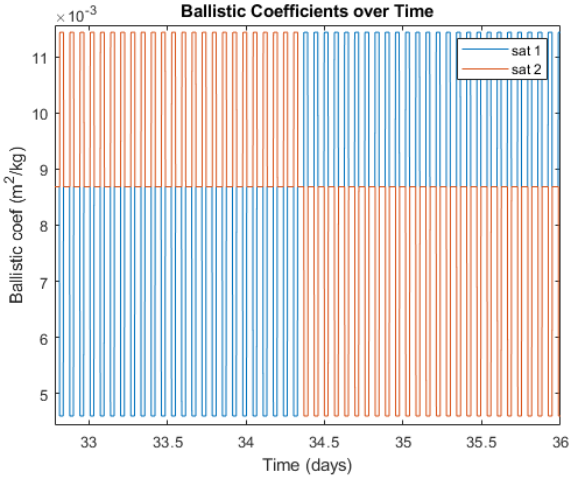

Figure 3. Zoomed in Ballistic Coefficients over Time during Differential Drag Maneuver

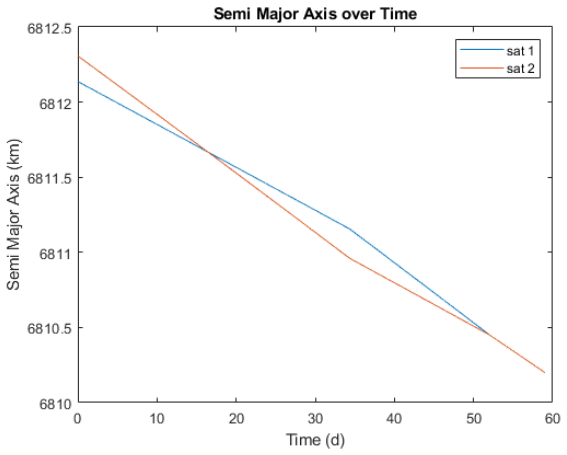

Figure 4. Semi Major Axis over Time during Differential Drag Maneuver with Two-Body Orbit

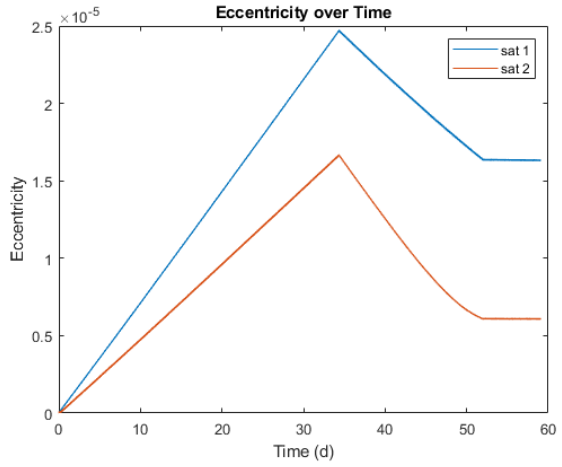

Figure 5. Eccentricity over Time during Differential Drag Maneuver with Two-Body Orbit

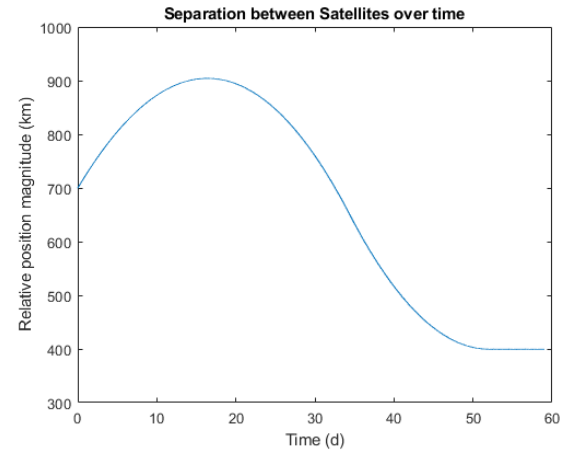

Figure 6. Separation over Time during Differential Drag Maneuver

As the Figure 2 illustrates, satellite 1 begins in a minimum drag configuration and sat 2 begins in a maximum drag configuration. As a result, the semi-major axis of satellite 2 drops more quickly than that of sat 1 due to aerodynamic decay as shown in Figure 4. When the semi-major axes of both satellites are at the same value, the rate of separation drops to zero as seen in Figure 6. As the semi-major axis of sat 2 continues to drop below that of sat 1, the rate of separation becomes negative. Because the ballistic coefficient swap time was accurately computed, both satellites arrive at the same semi-major axis when the desired separation change has been achieved and there is no drift after this. While holding a min or max drag state only in eclipse does induce some eccentricity, it is extremely tiny and is over an order of magnitude smaller than the eccentricity naturally induced by J2 perturbations. Figure 7, Figure 8, and Figure 9 show the separation, mean semi-major axis, and eccentricity respectively for a similar maneuver simulated in a high fidelity environment with gravitational perturbations from the EGM2008 model through degree and order 9 included. The large eccentricity oscillations are caused by J2 effects and are significantly larger than any eccentricity induced by differential drag maneuvering. In perturbed orbits, it is preferable to use mean orbital elements for computations, but even those will have some oscillations due to higher order gravitational terms.

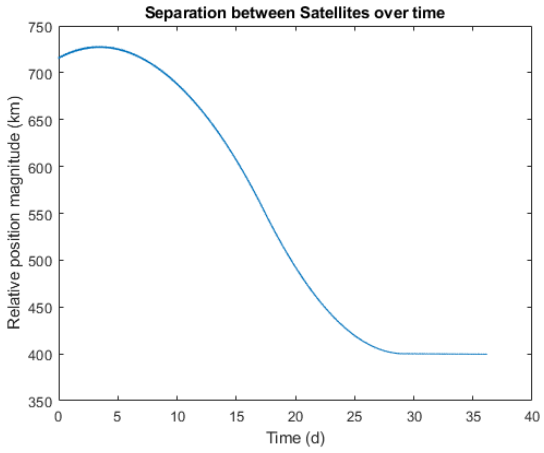

Figure 7. Separation over Time during Differential Drag Maneuver in High Fidelity Simulation Environment

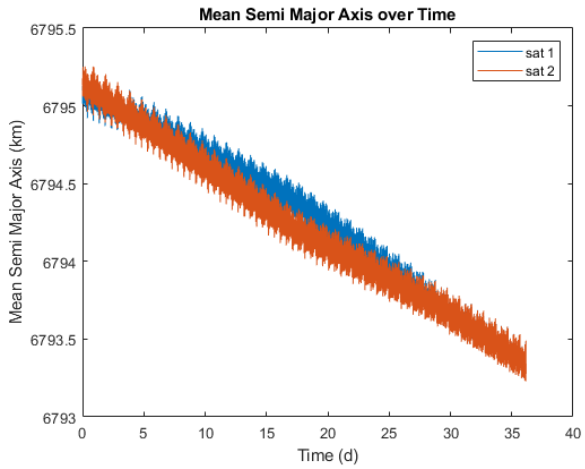

Figure 8. Mean Semi-major Axis over Time during Differential Drag Maneuver in High Fidelity Simulation Environment

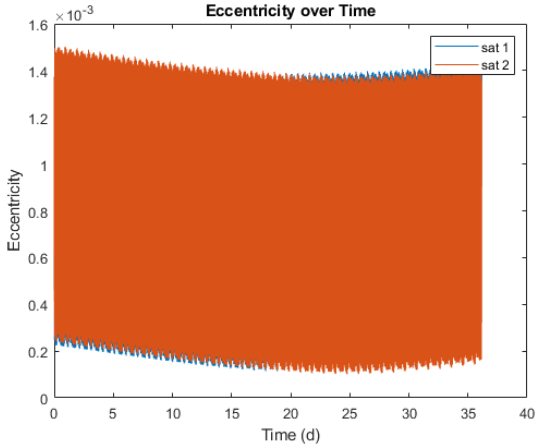

Figure 9. Eccentricity over Time during Differential Drag Maneuver in High Fidelity Simulation Environment

ON-ORBIT RESULTS FROM DIFFERENTIAL DRAG MANEUVER

During early mission operations, the SV1 and SV2 vehicles were observed to be drifting apart more quickly than expected after the deployment of SV2. SV1 was ahead of SV2 in the along-track direction and was at a lower mean semi-major axis, resulting in the increasing along-track separation over time. The decision was made to attempt to perform a differential drag maneuver to bring SV1 and SV2 closer together (target final separation of 400 km) and nullify the drift rate. To do this, SV1 was initially set to a minimum drag configuration and SV2 to a maximum drag configuration. At a swap time t_s, SV1 would be set to maximum drag and SV2 to minimum drag such that the desired final separation would be achieved when the satellites returned to the same mean semi-major axis at t_r. The differential drag maneuvering algorithms were re-run every several days using the latest states of each satellite to compute updated values of t_s and t_r. Initially, raw GPS ECI position and velocity were used for the satellite initial states. The inaccuracy on the initial GPS state was found to be one of the largest drivers of uncertainty in the computed t_s and t_r. As a result, future maneuver analysis was performed using estimated ECI position and velocity from an ephemeris filter onboard the satellite. The filtered state estimate was found to be significantly more accurate than raw GPS position and velocity. NORAD two-line elements (TLEs) were also found to be as accurate or more accurate than the filtered state estimate. Though TLEs are known for having errors on the order of several kilometers, the overwhelming majority of this error is in the along-track direction. As a result, a TLE-derived trajectory may have a larger initial position error, but the error generally will not grow as quickly as with a GPS-derived trajectory. Because of this and the ease of acquiring TLE estimates, t_s and t_r computation during the latter part of the maneuver was performed using TLE-derived initial state estimates. As in the example, both satellites were assumed to have a minimum and maximum ballistic coefficient of .00460 m^2/kg and .01143 m^2/kg respectively. Each satellite was assumed to be able to hold a minimum or maximum drag configuration only while in eclipse and maintain a sun-pointing configuration with an average ballistic coefficient of .00883 m^2/kg when in the sun. Table 1 shows the swap time and return time predictions based on initial conditions valid at the specified date.

Table 1. Initial Separation, Swap Time, and Estimated Return Time for 400 km Final Separation Maneuver for Different Sets of Initial Conditions

Initial conditions epoch	Estimated C_b swap date	Estimated maneuver completion date	Initial satellite separation (km)	Ephemeris source, density model
8/21/20	9/8/20	9/24/20	826	Raw GPS, best-fit exponential atmosphere
8/26/2020	9/4/2020	9/22/2020	858	Raw GPS, best-fit exponential atmosphere
8/31/2020	9/17/2020	10/06/2020	882	Raw GPS, NRLMSISE -00
9/3/2020	9/27/2020	10/20/2020	885.1	Filtered GPS, NRLMSISE-00
9/10/2020	9/27/2020	10/20/2020	872.4	Filtered GPS, NRLMSISE-00
9/17/2020 1700 UTC	9/27/2020 0400 UTC	10/21/2020 0500 UTC	832.7	Filtered GPS, NRLMSISE-00
9/20/2020 2000 UTC	10/3/2020, 1100 UTC	10/25/2020, 400 UTC	810	TLE, NRLMSISE-00
9/24/2020 1500 UTC	10/2/2020 2300 UTC	10/24/2020 1300 UTC	777.7	TLE, NRLMSISE-00
9/28/2020 0600 UTC	10/3/2020 0300 UTC	10/24/2020 1300 UTC	734.6	TLE, NRLMSISE-00
9/30/2020 1400 UTC	10/5/2020 0800 UTC	10/25/2020 0000 UTC	699.1	TLE, NRLMSISE-00
9/30/2020 2300 UTC	10/3/2020 1800 UTC	10/24/2020 1300 UTC	692.5	TLE, NRLMSISE-00

On 10/3/2020 0300 UTC, the vehicle drag configurations were switched such that SV1 was in max drag and SV2 was in min drag. Due to initial condition errors and uncertainties in the atmospheric model, we assumed the satellites likely would not achieve the desired 400 km separation perfectly at the time of return to the same semi-major axis if a differential drag state was maintained the entire time. If the satellites were on track to overshoot and achieve a final separation of less than 400 km, the error-minimizing technique would be to hold the differential drag state until the satellites converge to the same semi-major axis and then perform another maneuver to correct the remaining error. However, in an undershoot scenario where the satellites were projected to achieve a final separation greater than 400 km, a temporary "loiter" could be performed with both satellites in a minimum drag configuration. During this loiter, $\ddot{\phi}$ would be zero and ϕ would change at a constant rate $\dot{\phi}_0$ as given by Eq. (2) using the satellites' orbit-averaged mean semi-major axes at the start of the loiter. To determine whether a loiter is needed and compute loiter time, the change in mean argument of latitude separation if the satellites are brought to the same semi-major axis as fast as possible ($\Delta\phi_r$) is first computed via numerical simulation. A loiter is necessary only if $|\Delta\phi_r| < |\Delta\phi_{des}|$ where $\Delta\phi_{des}$ is the desired change in mean argument of latitude separation. In this case, the $\Delta\phi$ achieved with a loiter time of t_l prior to the return to a differential drag state is

$$\Delta\phi = \dot{\phi}_0 t_l + \frac{1}{2}\ddot{\phi} t_r^2 = \dot{\phi}_0 t_l + \Delta\phi_r \tag{27}$$

t_l can then be computed as

$$t_l = \frac{\Delta\phi_{des} - \Delta\phi_r}{\dot{\phi}_0} \quad (28)$$

Table 2 shows the expected final separation and maneuver completion date after the drag configuration swap assuming no loitering. If the final expected separation was greater than the 400 km, the suggested loiter time was computed. If the expected final separation was below 400 km, no loiter time was advised. The mission operators planned to implement a loiter if suggested loiter time exceeded several days. Because the actual drag force was smaller than expected, the maneuver took longer than expected to complete, forecasted final separation was soon less than 400 km, and no loiter was implemented on the satellites. All maneuver simulations were conducted using the NRLMSISE-00 density model, high fidelity gravity model, and TLE-derived initial conditions during this phase.

Table 2. Estimated Maneuver Completion Times and Separations at Different Initial Conditions during Second Phase of Drag Maneuver

Initial conditions valid time	Estimated maneuver completion date without loiter	Initial separation at epoch (km)	Estimated final separation without loiter(km)	Loiter time for 400 km final separation (days)
10/6/2020 2300 UTC	10/24/2020 2100 UTC	582.0	433.3	1.58
10/9/2020 0800 UTC	10/25/2020 0200 UTC	544.2	414.8	.82
10/12/2020 1900 UTC	10/28/2020 2100 UTC	493.7	300	0
10/14/2020 1300 UTC	10/25/2020 2300 UTC	469.2	376.5	0
10/14/2020 2100 UTC	10/25/2020 2200 UTC	464.9	376.5	0
10/19/2020 2000 UTC	10/26/2020 2300 UTC	404.9	361.0	0
10/22/2020 1300 UTC	10/29/2020 1600 UTC	374.6	332.1	0
10/23/2020 1300 UTC	10/28/2020 1200 UTC	365.4	343.5	0
10/25/2020 1700 UTC	11/1/2020 1600 UTC	347.4	311.0	0
10/26/2020 1800 UTC	10/27/2020 1100 UTC	340.5	339.7	0
10/27/2020 1400 UTC	10/31/2020 0000 UTC	333.7	323.6	0
10/29/2020 500 UTC	10/31/2020 1400 UTC	325.5	319.3	0
10/29/2020 1400 UTC	10/31/2020 1800 UTC	323.9	319.0	0

At 2300 UTC on Saturday, Oct 31 both satellites were placed in a minimum drag configuration. Satellite drift over time was monitored to assess the need for additional maneuvers. On 11/4/2020, a decision was made to put SV1 (the leader) in a max drag configuration between 11/5 2300 UTC and 11/7 2300 UTC in order to attempt to nullify the closure rate between the satellites of approximately 1.5 km/day. After this maneuver, the final separation between the satellite was 313 km with almost zero drift rate. This separation, though not the initial 400 km target, was deemed sufficient for mission operations and it was determined that an additional maneuver to achieve a precise 400 km separation was not needed. With both satellites in a minimum drag configuration, drift rate remained close to zero until the end of November. After this, satellite separation was periodically monitored to determine if any additional maneuvering was required. Figure 10 shows the separation between the satellites over time over the course of the differential drag maneuver using historical TLE data from Systems Toolkit (STK).

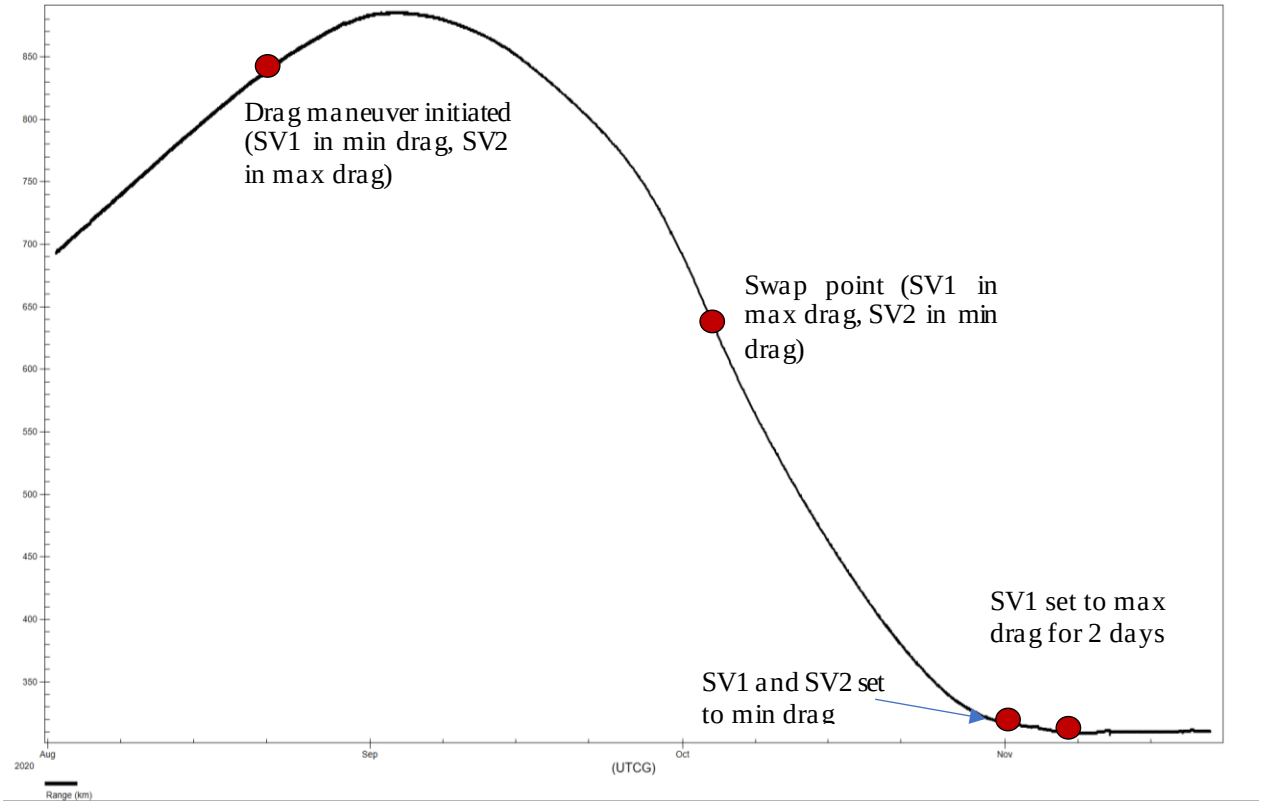

Figure 10. Separation over Time and Key Milestones during Differential Drag Maneuver

CONCLUSIONS

Simulation results and the in-flight experience from the Millennium Space Systems SV1 and SV2 vehicles demonstrates that the use of differential aerodynamics drag is an effective technique for controlling the along-track separation between two satellites. Use of a high-fidelity density model such as NRLMSISE-00 for drag-maneuver planning is important due to the significant variations in density that can occur in low Earth orbits. Even with the high-fidelity density model, maneuvering errors were caused by uncertainties in the spacecraft ballistic coefficients and the initial conditions. During the maneuvers performed, a-priori ballistic coefficient estimates were used. In future projects, it would be beneficial to estimate ballistic coefficients based on the observed orbital decay and use these estimates for maneuver planning. Additionally, the differential drag control algorithms would often return significantly different results when new initial conditions were provided simply due to ephemeris errors. Batch filtering of raw historical GPS data to get a more accurate initial state estimate would be beneficial for future projects. In the absence of accurate, batch filtered GPS data, TLEs are of sufficient accuracy for differential drag maneuvering and TLE-propagated trajectories generally have less long-term drift than trajectories propagated using a single GPS point. Occasionally, a TLE will have a larger than normal error and result in erroneous

maneuvering time computations. Changes in the drag configuration, especially in low orbits where drag is strong, often result in large initial TLE errors until the orbit estimators used to create the TLEs can accurately capture the new ballistic coefficient. In such cases, it is important to verify the results using several independent TLEs prior to changing satellite configurations. Despite the uncertainties and potential sources of error, differential drag is a viable means of orbit control for constellations of vehicles where rapid maneuvering and precise control are not critical. The use of differential drag makes spacecraft constellation control possible even for vehicles that do not contain thrusters.

REFERENCES

1. D. P. Scharf, F. Y. Hadaegh and S. R. Ploen, "A survey of spacecraft formation flying guidance and control. Part II: control," Proceedings of the 2004 American Control Conference, pp. 2976-2985 vol.4, doi: 10.23919/ACC.2004.1384365. 2004.
2. S. Iwasaki,T. Shibata,J. Nakamoto,H. Okamoto,H. Ishimoto,H. Kubota, "Characteristics of deep convection measured by using the A-train constellation," Journal of Geophysical Research, Vol. 11. 2010.
3. Palmerini, Giovanni & Sgubini, Silvano & Taini, Giacomo. Spacecraft Orbit Control using Air Drag. 56th International Astronautical Congress 10.2514/6.IAC-05-C1.6.10. 2005.
4. Omar, Sanny & Bevilacqua, Riccardo. Spacecraft Collision Avoidance Using Aerodynamic Drag. Journal of Guidance, Control, and Dynamics. 43. 1-7. 10.2514/1.g004518. 2019.
5. Foster, Cyrus, Henry Hallam, and James Mason. "Orbit determination and differential-drag control of Planet Labs CubeSat constellations." AIAA Astrodynamics Specialist Conference, Vale, OH, 2015.